



Chemical exfoliating of boron nitride into edge-hydroxylated nanosheets

Caifeng Chen¹, Chenkang Shao¹, and Andong Wang^{1,*}

¹School of Materials Science and Engineering, Jiangsu University, Zhenjiang 212013, Jiangsu, China

Received: 23 December 2022

Accepted: 15 February 2023

Published online:
27 February 2023

© The Author(s), under exclusive licence to Springer Science+Business Media, LLC, part of Springer Nature 2023

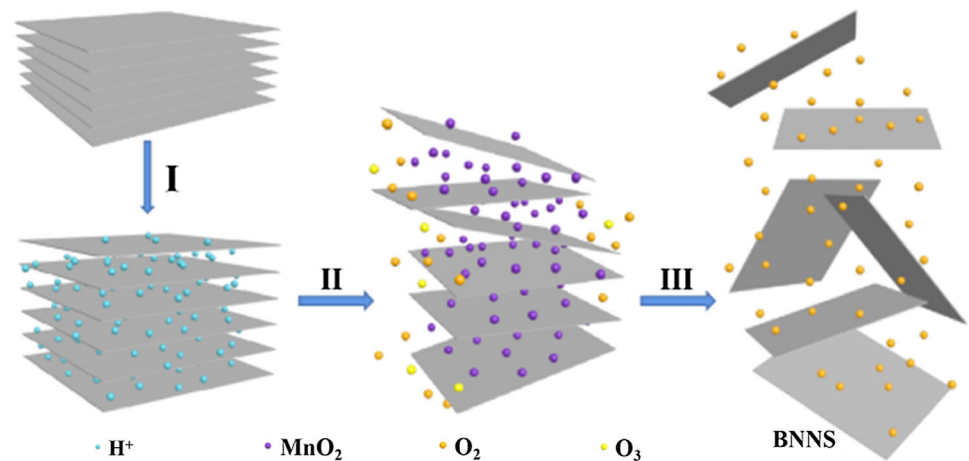
ABSTRACT

The edge-hydroxylated boron nitride nanosheets (BNNS) not only has excellent thermal stability, electrical properties, but also has high specific surface area, good dispersibility and compatibility. In this paper, edge-hydroxylated BNNS was obtained by stripping hexagonal boron nitride (h-BN) using wet chemical reaction method. The hydroxylated structure of the surface and formation mechanism of BNNS were analyzed, and the optimal controlled conditions were explored by orthogonal test. The results showed that the content of N element in the center of the BNNS (46.44 at. %) is significantly higher than that of B element in the edge of the sheets (33.10 at. %), and the content of O element in the edge of the sheets is nearly 30% higher than that in the center. It indicates that the edge of the BNNS introduces more oxygen than h-BN, the nitrogen atoms at the edge are replaced by oxygen atoms to achieve hydroxylation. When the mass ratio of h-BN and potassium permanganate is 1 g: 5 g, the reaction time is 9 h, and the reaction temperature is 60 °C, the obtained nanosheets have the best hydroxylation and good stripping effect. The average lateral size of the exfoliated nanosheets is 123 nm and only about three layers.

Handling Editor: Annela M. Seddon.

Address correspondence to E-mail: wadujs@163.com

GRAPHICAL ABSTRACT



Introduction

Boron nitride nanosheets (BNNS) is a two-dimensional layered material with hexagonal arrangement of graphene-like atoms [1]. It has high thermal conductivity, low thermal expansion and superior thermal stability [2, 3]. Its physical and chemical properties are extremely stable, and it has higher specific surface area and wide band gap than hexagonal boron nitride (h-BN). The hydroxylated BNNS also has excellent dispersibility and compatibility, and is easier to combine with other matrix materials and give full play to its performance. It has great application potential in the fields of electronic thermal conductive materials [4, 5], dielectric materials and sensors [6–8], fire retardant coatings and high temperature solid lubricants [9, 10].

Although the layered structure characteristics and lattice parameters are similar to those of graphene, the preparation method of BNNS are still very limited compared to graphene. This is mainly due to the fact that there is not only covalent bond but also partial ionic bond characteristics between B–N bonds, forming the interlaminar lip-lip effect, which makes the interlaminar force greater than the van der Waals force between graphite layers. Therefore, it is more

difficult to prepare single-layer or few-layer nanosheets than graphene [11].

At present, the preparation of BNNS can be carried out by bottom-up method and top-down method. Exfoliation remains the most promising method for the efficient preparation of monolayer or few-layer two-dimensional materials under low-cost, large-scale conditions. For example, Huang et al. [12] added h-BN powder to ethylene glycol, and then subjected to low power (100 W) ultrasonic treatment for 30 min to obtain a stable dispersion of BNNS as milky white colloid. Zhu et al. [13] first raised h-BN to 800 °C in air, and then immediately immersed it in liquid nitrogen until the liquid nitrogen was completely gasified. The thickness of BNNS stripped by this method is less than 5 atomic layers. Wang et al. [14] added polyvinyl pyrrolidone (PVP) to the ethanol/water mixture. After the PVP was completely dissolved, h-BN powder was added to form a dispersion, and the h-BN in the dispersion was stripped by carbon dioxide in a supercritical state (temperature 313.2 K, pressure 7.15 MPa). Deshmukh et al. [15] carried out green liquid exfoliation of h-BN using various plant extracts. The plant extract can be adsorbed on the surface of h-BN as a green surfactant to weaken the interaction between the boron nitride layers. The h-BN was slowly exfoliated by ultrasound at 40 kHz and 30 °C for 24 h, and the obtained BNNS

can be stably dispersed in water. Yaras et al. [16] developed a chemical exfoliation method. They stirred concentrated sulfuric acid, h-BN and potassium permanganate in a water bath at 25 °C for 30 min. The oxidation reaction of BN was completed by using deionized water and 30% (V/V) hydrogen peroxide solution to obtain nano-sized few-layer BNNS. Yu et al. presented a high-yield (+ 83%), low cost and energy-efficient wet chemical exfoliation strategy, which produces few-layers(3–6 layers) of edge-functionalized (OH) h-BN nanosheets with uniform size (486 ± 51 nm) [17]. The yield of BNNS by the chemical exfoliation method is high and effective. However, only a few studies have explored the optimized exfoliating conditions, and there is a lack of understanding of the conditions for chemical exfoliation of high-quality functionalized BNNS.

In this paper, h-BN was stripped by water bath chemical reaction to obtain edge-functionalized BNNS. The hydroxylated structure and formation mechanism of BNNS surface were analyzed, and the optimal controlled conditions were explored by orthogonal experiment.

Material and methods

10 mL of concentrated sulfuric acid (2 mol/L, $\geq 98.0\%$, Guoyao Reagent Company) was added to a conical flask containing 0.4 g h-BN (1 ~ 2 μm , Macklin) and mixed evenly. The conical flask was placed in an ice water bath, and a certain concentration of potassium permanganate (CP, $\geq 99.0\%$, Guoyao Reagent Company) was added slowly according to the ratio of raw materials. After the reaction was complete, the sealed conical flask was transferred to a water bath pot at 45 ~ 75 °C temperature for heating and stirring for 3 ~ 9 h. Subsequently, the conical flask was placed in an ice water bath, 20 mL of ice water was added, and 5 mL of hydrogen peroxide (GR, $\geq 30.0\%$, Guoyao Reagent Company) was slowly dripped. The suspension was collected with a centrifuge tube, and the deionized water and anhydrous ethanol were used for multiple washing and centrifugation (10000 rpm, 10 min) until the pH of the supernatant was 7. The precipitate obtained by centrifugation was dried in an oven (60 °C, 12 h) to obtain a white powdery BNNS sample.

The three main factors of mass ratio of h-BN and potassium permanganate (A), water bath reaction time (B), water bath reaction temperature (C) and three levels from each factor were selected to design orthogonal test for optimizing the preparation conditions. The factors and levels are shown in Table 1.

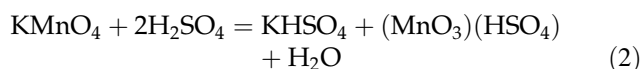
The morphology of the samples was observed by SEM (NovaNano450, FEI, USA) and transmission electron microscope (JEM-2100F, Japan). The element composition of BNNS was analyzed by X-ray photoelectron spectrometer (XPS, Shimadzu AXIS, Japan) and Octane Plus X-ray energy spectrometer (EDS, EDAX, Japan). The surface microstructure of BNNS was characterized by UV–Vis spectrophotometer (UV2600, Shimadzu, Japan), and Fourier transform infrared spectrometer with ATR mode (FT–IR, Nicolet iS50, USA). E_{2g} characteristic peaks of BNNS are measured by DXR laser micro-Raman spectrometer (Raman, Thermo Fisher, USA). The measuring range is 50–3393 cm^{-1} , and each sample is measured three times at different positions.

Results and discussion

The stripping process analysis of BNNS

Once potassium permanganate was added to the mixture of concentrated sulfuric acid and h-BN powder, a violent redox reaction took place. Figure 1 shows the color changes of the mixture after the reaction in water bath at 45 °C, 60 °C and 75 °C, respectively.

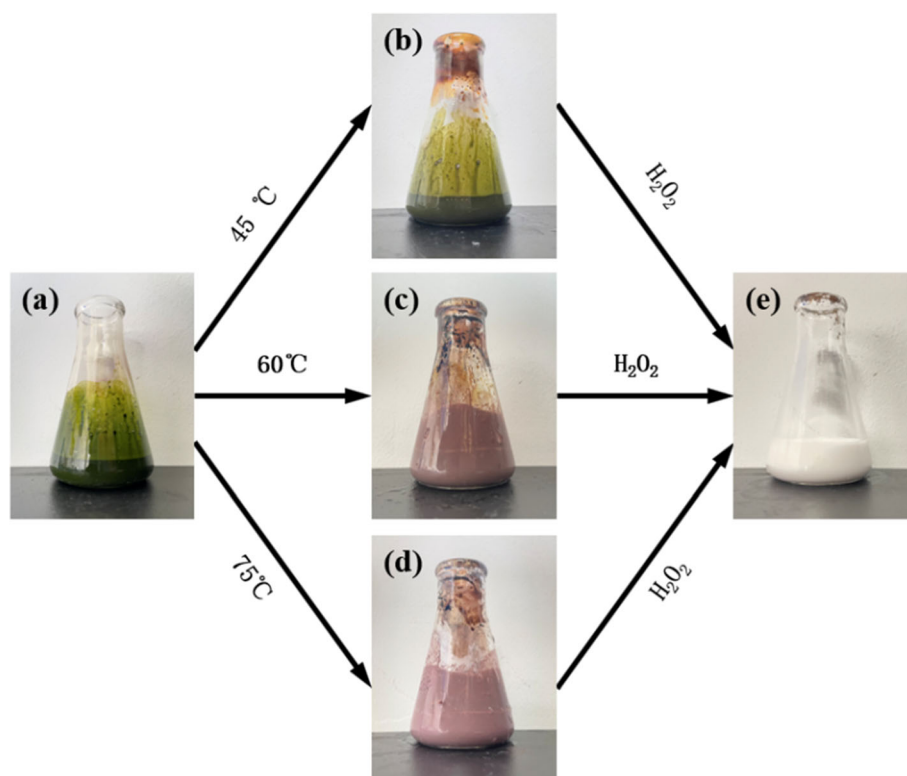
Before heating, concentrated sulfuric acid and potassium permanganate undergo a chemical reaction and become a green mixture, as shown in Fig. 1a. The dark green substance may be Mn_2O_7 or the mixture of MnO^{3+} and BN, the chemical reaction in this process is as follows:



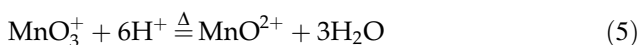
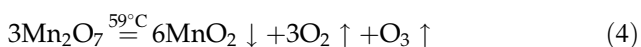
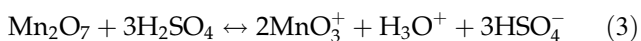
It can be seen from Fig. 1b that the color of the mixture did not change after heating at 45 °C, and it was still dark green without chemical reaction. However, after heating at 60 °C and 75 °C, the mixture changed from dark green to pink, as shown in Fig. 1c, d. This is because Mn_2O_7 will decompose

Table 1 Factors and levels in orthogonal test

Factors	(A) h-BN:KMnO ₄ (g:g)	(B) Time (h)	(C) Temperature (°C)
Level 1	(A1)1:1	(B1)3	(C1)45
Level 2	(A2)1:3	(B2)6	(C2)60
Level 3	(A3)1:5	(B3)9	(C3)75

Figure 1 Color change of the reaction mixture.

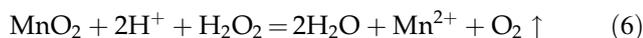
after heating above 59 °C, and it is easy to generate MnO_3^+ in concentrated sulfuric acid. Manganese ions with different valence states have different colors, only Mn^{2+} is pink. Therefore, the following reactions occurred.



When concentrated sulfuric acid and potassium permanganate encounter in a fierce chemical reaction, the generated energy will reduce the van der Waals force between the h-BN layers, and hydrogen ions take the opportunity to insert into the layered

BN and fill in the BN layers, as shown in the first step of Fig. 2. The MnO_2 particles generated by the water bath reaction were further inserted into the interlayer of the bulk h-BN, which expanded the interlayer spacing and prevented the re-accumulation of BNNS, as shown in the second step of Fig. 2. At the same time, the oxygen and ozone generated by the reaction can produce an outward thrust, which helped the separation of the layers.

The mixture was cooled sharply in ice water, and then hydrogen peroxide was added, the reaction showed violently exothermic. At this time, the color of the mixture became pure white (shown in Fig. 1e), and the manganese dioxide particles were removed under the action of hydrogen peroxide. The following reactions occurred:



The oxygen generated by the reaction spills out from the inside to the outside, creating a thrust, and the temperature difference generated by the ice bath also triggers the volume contraction of the lamellae and further loosening of the block, which eventually leads to complete detachment and formation of BNNS. The stripping process is shown in the third step of Fig. 2.

Surface morphology and microstructure analysis of BNNS

Figure 3a is the SEM microtopography of stacked h-BN crystal before stripping, and the TEM morphology of the stripped BNNS is shown in Fig. 3b. It

Figure 2 Schematic diagram of hydrothermal stripping mechanism of BNNS.

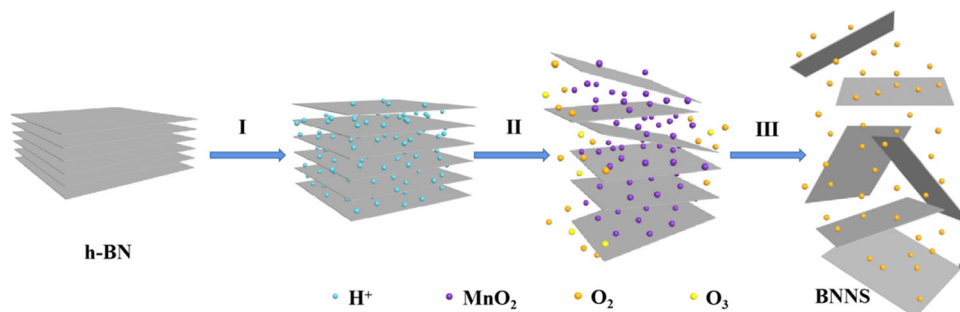
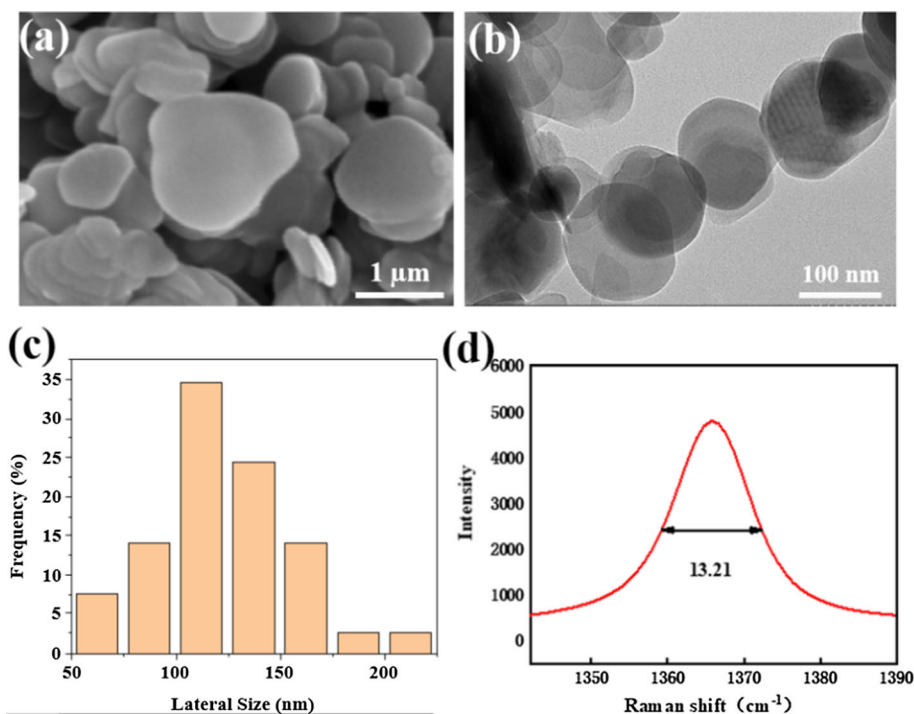


Figure 3 **a** SEM images of h-BN, **b** TEM images of BNNS **c** Size distribution of BNNS, **d** Raman spectroscopy of BNNS.



can be seen from the figure that after stripping, the BNNS is a sheet-like two-dimensional material with a graphene-like structure. The sheet is very flat, and no bending or folding of the nanosheets is observed, and there are no defects at the edges of the nanosheets, indicating that the chemical stripping has less damage to its shape. The average lateral size of BNNS is about 123 nm, and the particle size distribution is shown in Fig. 3c.

Figure 3d shows the Raman spectrum of BNNS, and its Raman characteristic peak has a sharp peak at 1365.75 cm^{-1} . Using Raman spectroscopy, the number of layers of nanosheets can be determined by Eq. (7) [18, 19]:

$$\langle N \rangle \text{vf} = [17.2 / (\Gamma_G - 8.5 - \log P)] - 1 \quad (7)$$

where, $\langle N \rangle_{vf}$ is the volume fraction weighted average number of BNNS layers, Γ_G is half-peak width of the characteristic peak, the unit is cm^{-1} , P is the laser power of the Raman spectrometer, here is 5mW. According to Eq. (7), the result is 3.29, namely, the number layer of BNNS is about 3.

Figure 4 shows the element distribution of BNNS obtained by SEM and energy spectrum analysis. As can be seen from the figure, nitrogen (N), boron (B) and oxygen (O) are widely distributed in the nanosheets.

To further confirm the distribution of each element in the center or edge of BNNS, EDS analysis was performed on BNNS. As shown in Fig. 5a, 1 ~ 4 are

the four points selected at the center of the-BNNS sheet, and 5 ~ 8 are the four points selected at the edge of the BNNS sheet.

Table 2 records the atomic percentage of N, B and O element at each point. It can be seen from the table that the content of B element in the center of the BNNS (50.55 at. %) is significantly lower than that in the edge (62.99 at. %). The content of N element in the center of the BNNS (46.44 at. %) is significantly higher than that of B element in the edge of the sheets (33.10 at. %). At the same time, the content of O element in the edge of the sheets (3.91 at. %) is nearly 30% higher than that in the center (3.01 at. %). The changes in the content of these elements and the

Figure 4 a Elemental analysis area of BNNS, and distribution maps of b B element, c N element, and d O element.

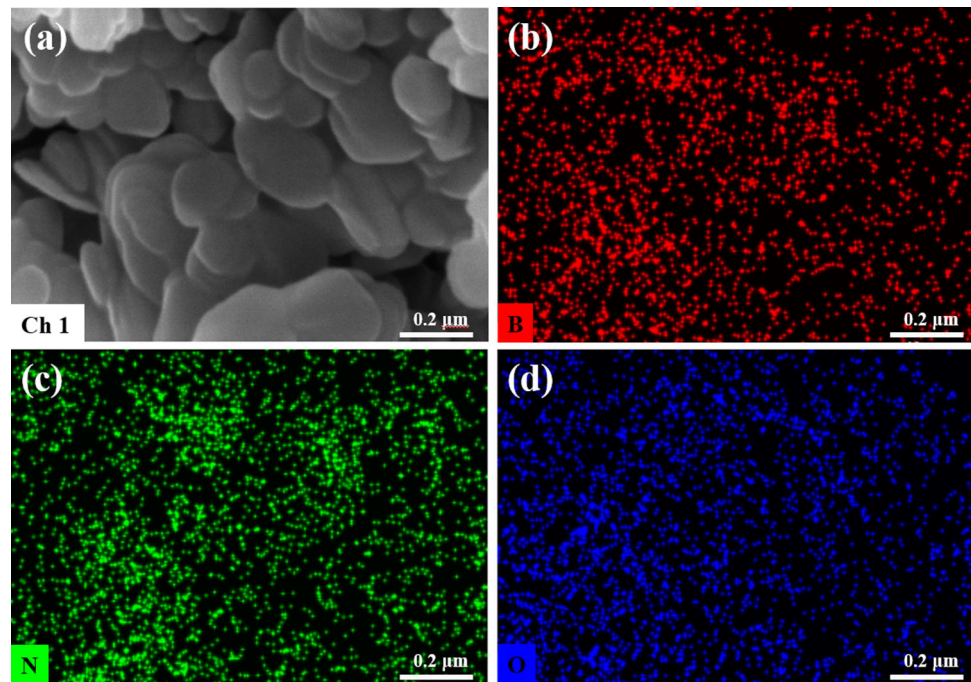


Figure 5 a Marked 1 ~ 8 in the image by scanning electron microscopy as the selection point for EDS analysis, b the structure diagram of edge hydroxylated BNNS.

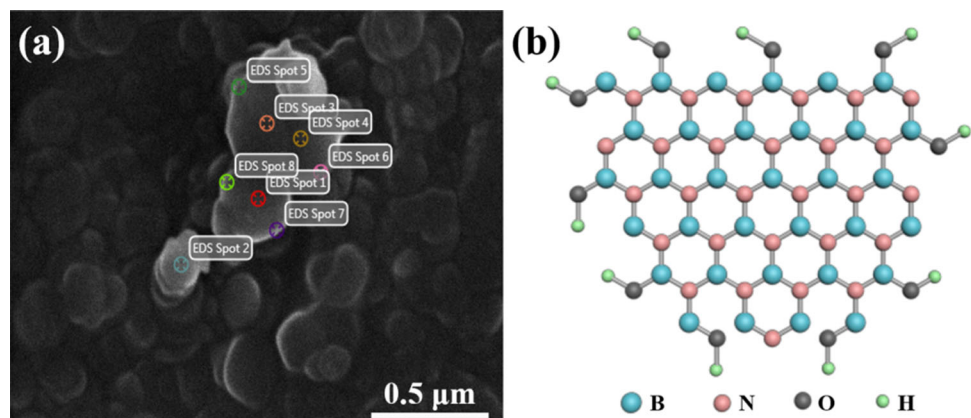
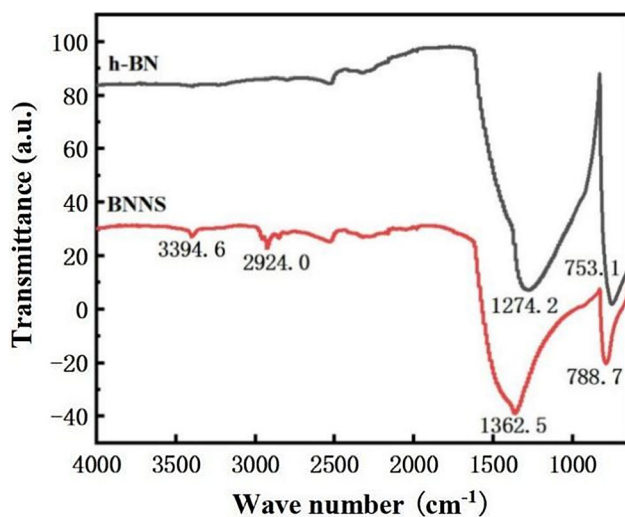


Table 2 EDS analysis of N, B, O content in the center and edge of BNNS

at. %	BNNS center					BNNS edge				
	1	2	3	4	Ave	5	6	7	8	Ave
B	47.52	50.25	51.86	52.56	50.55	64.16	65.07	63.34	59.40	62.99
N	49.58	47.41	45.03	43.74	46.44	31.62	31.28	32.83	36.67	33.10
O	2.90	2.34	3.11	3.7	3.01	4.21	3.65	3.83	3.93	3.91

appearance of oxygen are due to the strong redox reaction of concentrated sulfuric acid and potassium permanganate during the exfoliation of h-BN. In this intense reaction process, the B–N bond of h-BN is attacked by oxygen atoms. The oxygen atoms replace the nitrogen atoms and connect with the boron atoms, and further form O–H with the hydrogen ions filled in the interlayer, thus the element content changes, as shown in the schematic diagram of Fig. 5b. In addition, there are more exposed B–N bonds at the edge of the sheet than at the center, so the insertion of oxygen atoms tends to occur at the edge of the sheet, resulting in a significant decrease in nitrogen and an increase in oxygen at the edge of the sheet. It means that hydroxyl functionalization of BNNS is easily generated at the edge of the nanosheet.

Figure 6 is the FT-IR spectra of the samples before and after stripping. It can be seen from the diagram that h-BN has two characteristic peaks at 1274.2 cm^{-1} and 753.1 cm^{-1} , which represent the in-plane stretching vibration of B–N bond and the out-of-plane bending vibration of B–N–B, respectively. The spectrum of BNNS shows two peaks at 1362.5 cm^{-1} and 788.7 cm^{-1} , which also correspond to the in-

**Figure 6** FT-IR spectra of h-BN and BNNS.

plane stretching vibration of B–N bond and the out-of-plane bending vibration of B–N–B, respectively. In addition to these two peaks, the new absorption peaks appeared at 2924.0 cm^{-1} and 3394.6 cm^{-1} , which can be attributed to the water molecules adsorbed on the surface of BNNS and the introduction of –OH functional groups on the surface of BNNS after exfoliation (the –OH bonding peak is around 3400 cm^{-1}).

Surface hydroxylation analysis of BNNS

Figure 7 is the XPS spectra of h-BN and BNNS. It can be seen from the figure that h-BN and BNNS have boron (B1s) peaks near 190 eV, carbon (C1s) peaks near 284 eV, nitrogen (N1s) peaks near 398 eV, and oxygen (O1s) peaks near 533 eV. The presence of carbon in h-BN is due to the addition of carbon during the manufacturing process to suppress the crystal growth of h-BN to achieve an ideal particle size and increase the purity of the resulting h-BN [17]. After removing the interference of C element, the atomic percentages of O, N and B element and the N/B atomic ratio were calculated using XPS spectra, as shown in Table 3. From the table, the content of O element in the exfoliated samples increased from 8.44

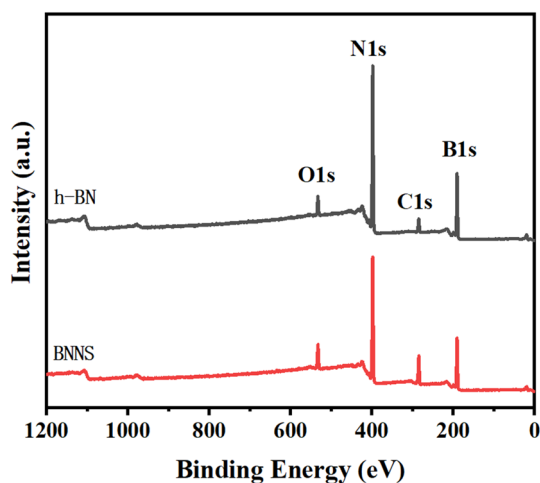
**Figure 7** XPS spectra of h-BN and BNNS.

Table 3 O, N, B atomic percentage and N/B of h-BN and BNNS

Sample	O (at.%)	N (at.%)	B (at.%)	N/B
h-BN	8.44	68.11	23.45	2.90
BNNS	13.00	63.69	23.31	2.73

at. % to 13.00 at. %, while the N/B atomic ratio decreased from 2.90 to 2.73. During the reaction, the oxygen atom replaces the connection between the nitrogen atom and the boron atom, which causes the formation of O–H with the hydrogen ion to increase the oxygen content and decrease the N/B atomic

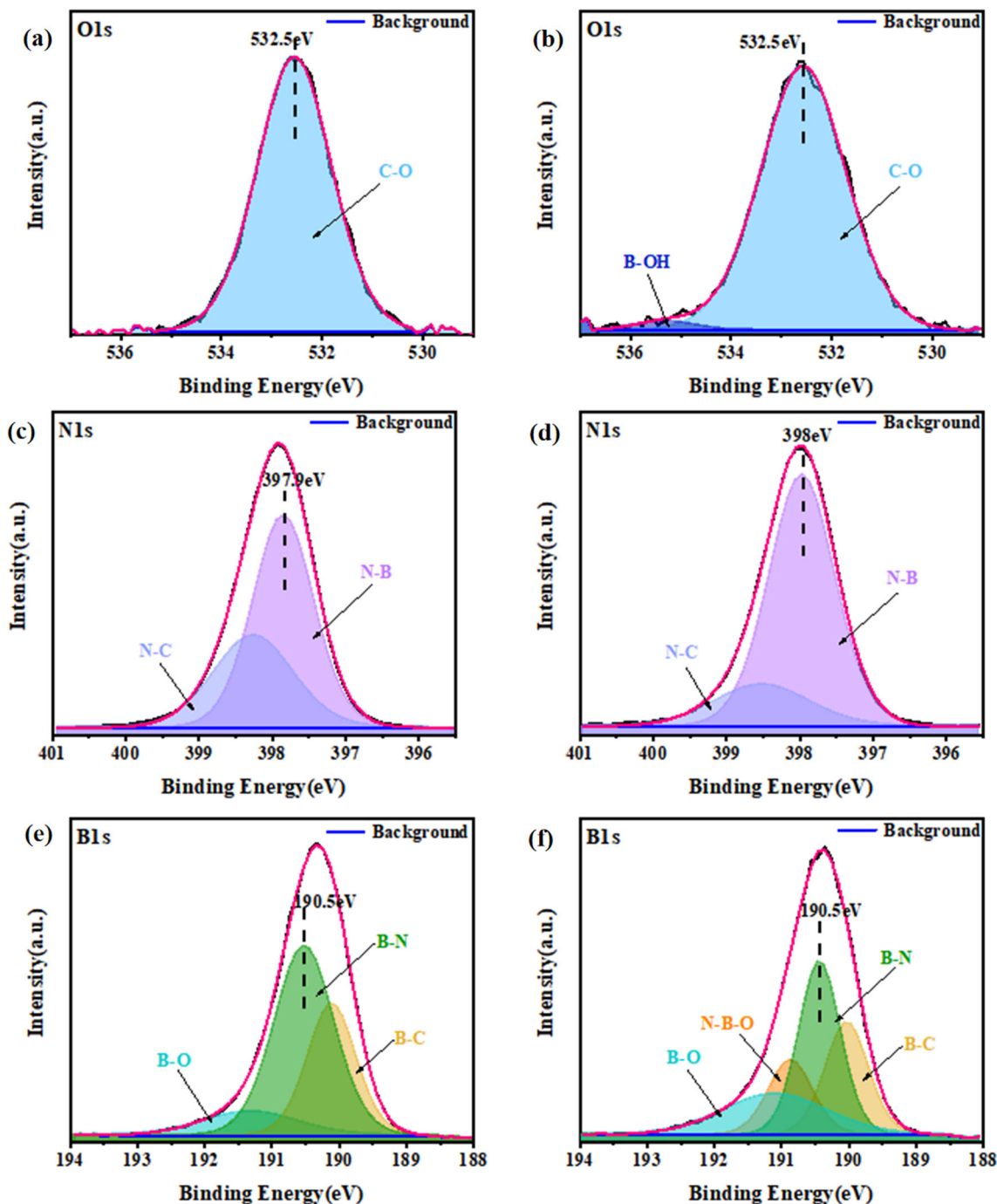


Figure 8 a O1s of h-BN; b N1s of BNNS; c N1s of h-BN; d N1s of BNNS; e B1s of h-BN; f N1s of BNNS.

ratio. This indicates that compared with h-BN, the oxygen content of the exfoliated BNNS increases and the nitrogen content decreases relatively.

The XPS spectra are fitted by peaks using Casa XPS, as shown in Fig. 8. The O1s spectrum of h-BN has only one C-O peak at about 532.50 eV (Fig. 8a), while BNNS has a B-OH peak at about 535.36 eV, as shown in Fig. 8b, which is caused by the hydroxylation of boron atoms at the edge of BNNS [17].

As can be seen from Fig. 8c, d, the N1s spectra of h-BN and BNNS have two peaks at 398.00 eV and 398.50 eV, corresponding to N-B and N-C peaks, respectively [20]. The B1s spectra in Fig. 8e, f show that h-BN and BNNS are mainly composed of B-N bonds at 190.50 eV, followed by B-C bonds at about 190.00 eV [21]. h-BN has a B-O peak at about 191.20 eV [22], which is due to the adsorption of oxygen molecules on the surface of the sample. In addition to the B-O peak, BNNS has a N-B-O peak at about 190.86 eV, which indicates that BNNS introduces more oxygen than h-BN, which is caused by the hydroxylation of some boron atoms on the surface of the sample.

Optimization analysis of preparing conditions for hydroxylation

Table 4 is a nine-group experimental scheme designed by $L_9(3^4)$ orthogonal test, and the O element content of the samples detected by EDS is used as an

indicator to optimize the preparation conditions for hydroxylation.

As may be seen from Table 4, the oxygen content of the samples obtained under different preparation conditions is different. Where, K refers to the sum of the indexes of the orthogonal test corresponding to the level of each factor; k is the average value of K, and R is the difference between the maximum and minimum value in K value. From the analysis of the orthogonal test results, it can be seen that the order of range value is $R(C) > R(A) > R(B)$, which indicates that factor C (water bath reaction temperature) has the strongest influence, followed by A (the mass ratio of h-BN and potassium permanganate) and then B (water bath reaction time). Comparing the K_i (or k_i) of each column, the optimal scheme should be A3B3C2, which is also known as scheme 7. Therefore, when the mass ratio of h-BN and potassium permanganate is 1 g: 5 g, the reaction time is 9 h, and the reaction temperature is 60 °C, the O element content of the obtained BNNS is up to 3.11 at. %.

Figure 9 shows the UV-Vis spectra of stripped BNNS obtained by nine different schemes. As may be seen from the figure, h-BN has an only strong absorption peak [19]. However, the exfoliated BNNS showed new absorption peaks around 213 nm and 280 nm, which were formed by the addition of oxygen atoms/hydroxyl groups. The new absorption peaks of BNNS obtained in scheme 7 is the most

Table 4 Results and analysis of $L_9(3^4)$ orthogonal test

number	A(g:g)	none	B(h)	C(°C)	O (at.%)
1	1:1		3	45	1.44
2	1:1		6	60	2.72
3	1:1		9	75	0.94
4	1:3		6	75	1.06
5	1:3		9	45	1.48
6	1:3		3	60	1.20
7	1:5		9	60	3.11
8	1:5		3	75	1.24
9	1:5		6	45	1.47
K_1	5.10	5.61	3.88	4.39	
K_2	3.74	5.44	5.25	7.03	
K_3	5.82	3.61	5.53	3.24	
k_1	1.70	1.87	1.29	1.46	
k_2	1.25	1.81	1.75	2.34	
k_3	1.94	1.20	1.84	1.08	
Range(R)	2.08	2.00	1.65	3.79	
Main factor → secondary	C A B				
Optimal scheme	A3B3C2				

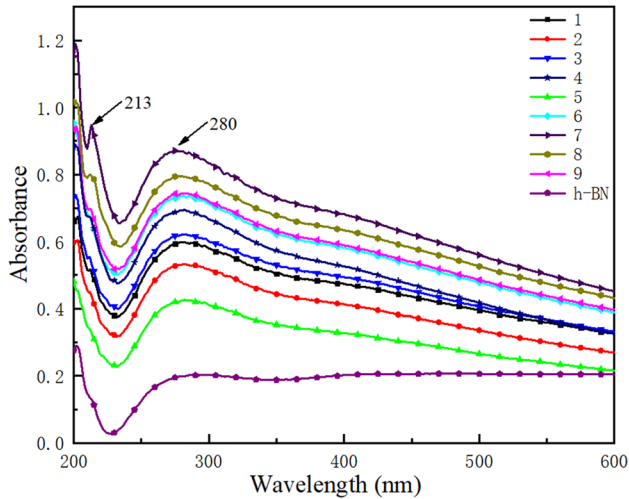
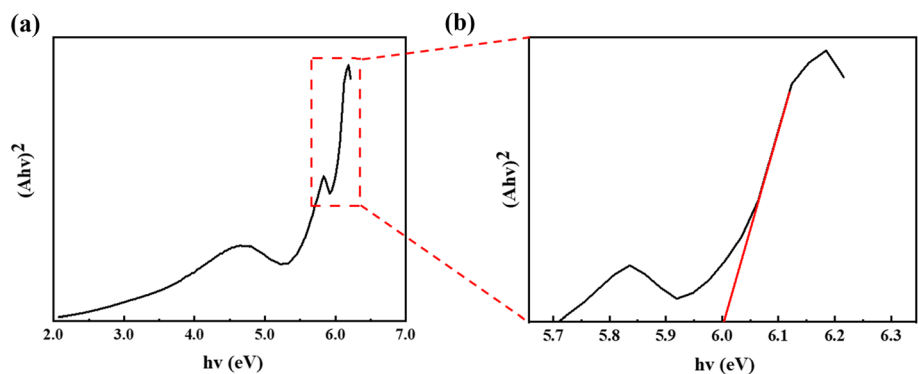


Figure 9 UV-Vis spectra of h-BN and BNNS by stripping with schemes 1 ~ 9.

obvious, which confirms that the surface hydroxylation of BNNS is obvious. In addition, according to Beer-Lambert law [23], the absorption intensity of light at a certain wavelength is proportional to the concentration of the substance. Therefore, a higher UV absorption value indicates a higher concentration of BNNS dispersion, which means a higher yield of BNNS. Compared with other groups of schemes, the results in the figure show that scheme 7 should have the highest yield.

The Tauc plot drawn from the UV-Vis spectra can be used to determine the optical band gap of BNNS [24]. Figure 10a shows the Tauc plot of the BNNS stripped using the optimal scheme 7. The straight line in Fig. 10b is extended and intersected with the X-axis at about 6.0 eV, which is consistent with the literature report [25], indicating that the BNNS stripped under this condition is a few-layer nanosheet.

Figure 10 Tauc diagram of BNNS prepared by stripping with schemes 7.



In summary, the BNNS prepared by scheme 7 not only has obvious surface hydroxylation, but also has the characteristics of few-layers and higher yield. It is the optimal scheme for the preparation of partially hydroxylated BNNS by stripping.

Conclusions

In summary, the edge-hydroxylated BNNS was successfully obtained by controlled exfoliation of hexagonal boron nitride (h-BN). During the wet chemical reaction process, the strong reaction of concentrated sulfuric acid and potassium permanganate causes H^+ to insert into the interlayer of the layered material, and the B-N bond of h-BN is attacked by oxygen atoms. The oxygen atoms replace the nitrogen atoms to connect with the boron atoms and form O-H with the hydrogen ions filled in the interlayer. Compared with h-BN, BNNS introduces more oxygen atoms than h-BN, and some nitrogen atoms at the edge are replaced by oxygen atoms to achieve hydroxylation. When the mass ratio of h-BN and potassium permanganate is 1 g: 5 g, the reaction time is 9 h, and the reaction temperature is 60 °C, the obtained nanosheets have the best hydroxylation and good stripping effect. The average lateral size of the exfoliated nanosheets is about 123 nm, the number of layers is about 3, and the optical band gap is about 6.0 eV. This material has high specific surface area and excellent dispersibility, and has potential application prospects in the preparation and application of high-performance composite materials.

Acknowledgements

This work was supported by the National Natural Science Foundation of China (No. 52175464).

Author contributions

AW and CC performed the experimental design and data analysis; CS completed the data collection; CC wrote the manuscript.

Data availability

All data included in this study are available upon request by contact with the corresponding author.

Declarations

Conflicts of interest The authors declare that they have no conflict of interest.

References

- [1] Pakdel A, Zhi C, Bando Y, Golberg D (2012) Low-dimensional boron nitride nanomaterials. *Mater Today* 15:256–265. [https://doi.org/10.1016/S1369-7021\(12\)70116-5](https://doi.org/10.1016/S1369-7021(12)70116-5)
- [2] Wang Y, Xu L, Yang Z, Xie H, Jiang P, Dai J, Luo W, Yao Y, Hitz E, Yang R, Yang B, Hu L (2018) High temperature thermal management with boron nitride nanosheets. *Nanoscale* 10:167–173. <https://doi.org/10.1039/C7NR07058F>
- [3] Kostoglou N, Polychronopoulou K, Rebholz C (2015) Thermal and chemical stability of hexagonal boron nitride (h-BN) nanoplatelets. *Vacuum* 112:42–45. <https://doi.org/10.1016/j.vacuum.2014.11.009>
- [4] Wang Z, Meng G, Wang L, Tian L, Chen S, Wu G, Kong B, Cheng Y (2021) Simultaneously enhanced dielectric properties and through-plane thermal conductivity of epoxy composites with alumina and boron nitride nanosheets. *Sci Rep* 11:2495. <https://doi.org/10.1038/s41598-021-81925-x>
- [5] Wang T, Zhang G, Zhang B, Liu S, Li D, Liu C (2021) Oriented boron nitride nanosheet films for thermal management and electrical insulation in electrical and electronic equipment. *ACS Appl Nano Mater* 4:4153–4161. <https://doi.org/10.1021/acsanm.1c00484>
- [6] Wu L, Wu K, Lei C, Liu D, Du R, Chen F, Fu Q (2019) Surface modifications of boron nitride nanosheets for poly(vinylidene fluoride) based film capacitors: advantages of edge-hydroxylation. *J Mater Chem A* 7:7664–7674. <http://doi.org/10.1039/C9TA00616H>
- [7] Kim KB, Jang W, Cho JY, Woo SB, Jeon DH, Ahn JH, Hong SD, Koo HY, Sung TH (2018) Transparent and flexible piezoelectric sensor for detecting human movement with a boron nitride nanosheet (BNNS). *Nano Energy* 54:91–98. <https://doi.org/10.1016/j.nanoen.2018.09.056>
- [8] Atar N, Yola ML (2018) Core-shell nanoparticles/two-dimensional (2D) hexagonal boron nitride nanosheets with molecularly imprinted polymer for electrochemical sensing of cypermethrin. *J Electrochem Soc* 165:H255–H262. <https://doi.org/10.1149/2.1311805jes>
- [9] Gan W, Chen C, Wang Z, Pei Y, Ping W, Xiao S, Dai J, Yao Y, He S, Zhao B, Das S, Yang B, Sunderland PB, Hu L (2020) Fire-resistant structural material enabled by an anisotropic thermally conductive hexagonal boron nitride coating. *Adv Funct Mater*. 1909196. <https://doi.org/10.1002/adfm.201909196>
- [10] Rasul MG, Kiziltas A, Arfaei B, Shahbazian-Yassar R (2021) 2D boron nitride nanosheets for polymer composite materials. *NPJ 2D Mater Appl*. 5(56):1-18. <https://doi.org/10.1038/s41699-021-00231-2>
- [11] Luo W, Wang Y, Hitz E, Lin Y, Yang B, Hu L (2017) Solution processed boron nitride nanosheets: synthesis, assemblies and emerging applications. *Adv Funct Mater* 27:1701450. <https://doi.org/10.1002/adfm.201701450>
- [12] Huang C, Chen C, Ye X, Ye W, Hu J, Xu C, Qiu X (2013) Stable colloidal boron nitride nanosheet dispersion and its potential application in catalysis. *J Mater Chem A* 1:12192–12197. <https://doi.org/10.1039/C3TA12231J>
- [13] Zhu W, Gao X, Li Q, Li H, Chao Y, Li M, Mahurin SM, Li H, Zhu H, Dai S (2016) Controlled gas exfoliation of boron nitride into few-layered nanosheets. *Angew Chem Int Edit* 55:10766–10770. <https://doi.org/10.1002/ange.201605515>
- [14] Wang N, Xu Q, Xu S, Qi Y, Chen M, Li H, Han B (2015) High-efficiency exfoliation of layered materials into 2D nanosheets in switchable CO₂/Surfactant/H₂O system. *Sci Rep* 5:16764. <https://doi.org/10.1038/srep16764>
- [15] Deshmukh AR, Jeong JW, Lee SJ, Park GU, Kim BS (2019) Ultrasound-assisted facile green synthesis of hexagonal boron nitride nanosheets and their applications. *ACS Sustain Chem Eng* 7:17114–17125. <https://doi.org/10.1021/acssuschemeng.9b03387>
- [16] Yaras A, Er E, Çelikkan H, Disli A, Alicilar A (2016) Cellulosic tent fabric coated with boron nitride nanosheets. *J Ind Text* 45:1689–1700. <https://doi.org/10.1177/1528083715569375>
- [17] Yu L, Yap PL, Tran DNH, Santos AMC, Losic D (2021) High-yield preparation of edge-functionalized and water dispersible few-layers of hexagonal boron nitride (hBN) by

- direct wet chemical exfoliation. *Nanotechnology* 32:405601. <https://doi.org/10.1088/1361-6528/ac0931>
- [18] Mahanta T, Mohanty T (2021) Fermi level modulation of boron nitride nanosheets by vacancy driven compressive strain. *Appl Phys Lett* 119:091902. <https://doi.org/10.1063/5.0051405>
- [19] Griffin A, Harvey A, Cunningham B, Scullion D, Tian T, Shih CJ, Gruening M, Donegan JF, Santos EJG (2018) Spectroscopic size and thickness metrics for liquid-exfoliated h-BN. *Chem Mater* 30:1998–2005. <https://doi.org/10.1021/acs.chemmater.7b05188>
- [20] Rastogi PK, Sahoo KR, Thakur P, Sharma R, Bawari S, Podila R, Narayanan TN (2019) Graphene-hBN non-van der waals vertical heterostructures for four-electron oxygen reduction reaction. *Phys Chem Chem Phys* 21:3942–3953. <https://doi.org/10.1039/C8CP06155F>
- [21] Sudeep PM, Vinod S, Ozden S, Sruthi R, Kukovec A, Konya Z, Vajtai R, Anantharaman MR, Ajayan PM, Narayanan TN (2015) Functionalized boron nitride porous solids. *RSC Adv* 5:93964–93968. <https://doi.org/10.1039/C5RA19091F>
- [22] Qu J, Li Q, Luo C, Cheng J, Hou X (2018) Characterization of flake boron nitride prepared from the low temperature combustion synthesized precursor and its application for dye adsorption. *Coatings* 8:214. <https://doi.org/10.3390/coatings8060214>
- [23] Oshina I, Spigulis J (2021) Beer-Lambert law for optical tissue diagnostics: current state of the art and the main limitations. *J Biomed Opt* 26:100901. <https://doi.org/10.1117/1.JBO.26.10.100901>
- [24] Tauc J (1968) Optical properties and electronic structure of amorphous Ge and Si. *Mater Res Bull* 3:37–46. [https://doi.org/10.1016/0025-5408\(68\)90023-8](https://doi.org/10.1016/0025-5408(68)90023-8)
- [25] Han R, Liu F, Wang X, Huang M, Li W, Yamauchi Y, Sun X, Huang Z (2020) Functionalised hexagonal boron nitride for energy conversion and storage. *J Mater Chem A* 8:14384–14399. <https://doi.org/10.1039/D0TA05008C>

Publisher's Note Springer Nature remains neutral with regard to jurisdictional claims in published maps and institutional affiliations.

Springer Nature or its licensor (e.g. a society or other partner) holds exclusive rights to this article under a publishing agreement with the author(s) or other rightsholder(s); author self-archiving of the accepted manuscript version of this article is solely governed by the terms of such publishing agreement and applicable law.